JTTEE5 16:933–939
DOI: 10.1007/s11666-007-9094-8
1059-9630/$19.00 © ASM International

Detection of Wear in One-Cathode Plasma Torch Electrodes and its Impact on Velocity and Temperature of Injected Particles

Georg Mauer, José-Luis Marqués-López, Robert Vaßen, and Detlev Stöver

(Submitted February 26, 2007; in revised form June 22, 2007)

Wear at the electrode surfaces of a one-cathode plasma torch changes the characteristic fluctuation pattern of the plasma jet. This affects the trajectory of the particles injected into the plasma jet in a non-controllable way, which degrades the reproducibility of the process. Time-based voltage measurements and Fourier analysis were carried out on a one-cathode F4 torch at different wear conditions to determine the evolution of wear dependant characteristics. A significant correlation is observed between increasing torch wear and decreasing voltage roughness and high frequency noise. Furthermore, by means of particle diagnostic systems, the change in the particle velocity and temperature has been measured. The variations of the particle characteristics are significant and thus an influence on the sprayed coating microstructure is to be expected.

Keywords electrode, particle diagnostics, plasma spraying, process monitoring, torch, voltage, wear

1. Introduction

Plasma spraying is a well-established process to manufacture coatings. Powder particles, suspended in a carrier gas, are injected into a plasma jet, generated within the plasma torch by an electric arc discharge. The particles, after being melted and accelerated in the plasma, impact onto the substrate to form individual lamellae, the stacking of which forming the coating. One-cathode plasma torches are widely used, wherein the arc is generated between a centered cathode and a coaxial cylindrical anode. The plasma gas is axially injected along the cathode tip and thus the arc segment connecting its central core to the anode wall is exposed to the transverse gas flow.

The formation and behavior of the arc have been intensively investigated (Ref 1). The instantaneous arc morphology and the time-dependent voltage waveform are found to be strongly correlated to each other. This allows investigating the arc performance by analyzing the torch voltage fluctuations. The arc core dynamics are particularly dependent on the plasma gas flow rate and composition as well as on the arc current. Three basic dynamic modes of the arc operation can be defined (Ref 2): with an increasing mean voltage, from a nearly constant voltage (steady mode), passing through a sinusoidal waveform of low amplitudes (takeover mode) up to the random, intensively fluctuating restrike mode. These operating modes are correlated with the thickness and the temperature of the cold-gas boundary layer between the arc and the anode nozzle wall. Anode wear is studied in Ref 2 showing that it leads to a thinner boundary layer and a reduced motion of the arc root. In Ref 3 it has been found, that in a one-cathode torch and for the considered all argon gas flows, those arc fluctuations of low frequency (100 and 300 Hz) are mainly caused by the rectification of the power supply, with higher frequency fluctuations at about 4 kHz, but with lower amplitude superimposed to the signal. In contrast, using nitrogen as secondary plasma gas, the influence of the arc restrike mode dominates the voltage waveform.

Arc fluctuations affect the performance of the plasma jet and thus the in-flight characteristics of the injected particles. In Ref 4 time resolved diagnostic measurements of the individual particle velocities and temperatures were carried out and correlated to the instantaneous voltage difference between the electrodes. The time-dependent variations in particle temperature and velocity due to the power fluctuation induced by the arc movements were found to be very large when plasma torch operates under restrike mode ($\Delta p/p \approx 100\%$). When operating under take over mode, those fluctuations decrease but still remain fairly large ($\Delta p/p \approx 30\%$). So the arc dynamics are a prime source of broadening the distribution of particle in-flight characteristics. As a consequence the deposition rate and the microstructure of the sprayed coating are affected.

This article is an invited paper selected from presentations at the 2007 International Thermal Spray Conference and has been expanded from the original presentation. It is simultaneously published in *Global Coating Solutions, Proceedings of the 2007 International Thermal Spray Conference*, Beijing, China, May 14-16, 2007, Basil R. Marple, Margaret M. Hyland, Yuk-Chiu Lau, Chang-Jiu Li, Rogerio S. Lima, and Ghislain Montavon, Ed., ASM International, Materials Park, OH, 2007.

Georg Mauer, José-Luis Marqués-López, Robert Vaßen, and **Detlev Stöver**, Institut für Energieforschung IEF-1, Forschungszentrum Jülich GmbH, 52425, Jülich, Germany. Contact e-mail: g.mauer@fz-juelich.de.

Thus a higher jet fluctuation leads to an increased porosity, a higher content of partially or not melted particles as well as to lower deposition rates (Ref 5). In Ref 6 correlations between torch power, arc root fluctuations and in-flight particle characteristics were identified operating the process at constant current. However, these latter results were assessed to be still not sufficient for an accurate control of the spray process.

Not only the time-dependent voltage waveform, but also its spectra in the frequency domain were used to obtain characteristic values of the wear state in torch electrodes. The comparison of the voltage evolutions in the time domain of a new and an eroded anode (Ref 7) shows decreasing standard deviations and shallower sawtooth shape profiles in the worn state. Variances of the peaks between 5 and 11 kHz are observed when operation conditions (plasma gases, current) are changed or when the anode is eroding. But the effects thereby modifying such peaks could not be clarified completely. In Ref 8 is shown that the time-dependent evolutions of the mean voltage display a steady light decrease followed by a sharp drop and unstable course after fatal erosion has occurred. In the frequency domain three peaks between 4 and 9 kHz are observed. With cumulating ignitions increasing amplitudes of the first and the third peak are observed and mainly correlated with cathode effects. A second long-term experiment with fewer ignitions shows a frequency shift of the first peak, which is assigned to anode wear. Generally the observed peaks give only slight response on increasing electrode wear. Only final catastrophic erosion might be detectable on this basis.

Frequency and amplitudes of the voltage spectra peaks in the range of 4 and 11 kHz (in the following called main peaks) are significantly determined by the plasma gas flow rate and composition as well as the electrodes geometry (Ref 7). This complicates accurate wear detection and process monitoring using spectra analysis in this frequency range.

In the present paper, an alternative way is presented: instead of considering the main peaks, the high frequency range (above 20 kHz) is investigated. It is found that the evolution of this range can be closely correlated to the macroscopic motion of the arc root along the anode surface, and thus characterizes the wear of the latter.

2. Time-Based Voltage Measurements and Power Spectra Analysis

Experiments were conducted on an A3000 atmospheric plasma spraying facility equipped with a one-cathode F4 gun (Sulzer Metco AG, Wohlen, Switzerland). For each experiment the torch electric efficiency η was estimated by the measurement of the temperature change between output and input of the known mass flow of cooling water. By means of a digital oscilloscope connected to a personal computer, series of $N = 2^{11} = 2048$ consecutive voltage values ΔV_i were measured, with a time resolution of $\Delta t = 2$ µs.

After a previous investigation of the influence on fluctuations by plasma gas diatomic species (H_2 and N_2), mass flow and electric current, the three cases of Table 1 were selected. The measured efficiency is $\eta \approx 60\%$ for the three cases. The evolution of each case has been tracked for a new torch (anode and cathode) and after 5, 10, 15, 20, 25, and above 25 h of operation, the latter denoted ''very worn'' hereafter. The number of ignitions was, respectively, 1, 14, 19, 23, 28, 40, and above 43.

Table 1 Considered spraying cases (gas species, mass flow, and electric current)

Case	Gas flow, slpm	Current, A	Total flow rate, slpm	H_2 or N_2 fraction
1	50.0/8.0 Ar/H_2	500	58.0	0.160
2	50.0/11.2 Ar/N_2	500	61.2	0.224
3	30.0/11.2 Ar/N_2	300	41.2	0.373

At each wear stage the three considered cases were measured consecutively. After visual inspection, the erosion on the anode was more developed than on the cathode (due in part to the lower total number of torch ignitions, 45, during the investigation). Therefore, the main torch wear will refer to the anode for the following. Actually the largest anode erosion is to be expected for the case with H_2 (case 1), due to the strongest plasma core constriction and the resulting higher power density (Ref 9). The two other cases with N_2 have been selected for investigating if the erosion already created under case 1 can also be detected when using other gas species.

For each time-voltage series measured a standard Fast Fourier Transform (FFT) was carried out (Ref 10). For the time resolution $\Delta t = 2$ µs, at each frequency ω

$$\omega = i\frac{2\pi}{N\Delta t} \quad (i = 1, \ldots, N/2 = 1024) \qquad \text{(Eq 1)}$$

the sum of the squared cosine component and squared sine component of the FFT is determined: the resulting function of ω is called the power spectrum $S(\omega)$ and it will be represented double logarithmically. Also the mean voltage ΔV_{ave} as well as the voltage roughness R_a are calculated for each series according to

$$\Delta V_{ave} = \frac{1}{N}\sum_{i=1}^{N}\Delta V_i\,, \quad R_a = \frac{1}{N}\sum_{i=1}^{N}|\Delta V_i - \Delta V_{ave}| \qquad \text{(Eq 2)}$$

where ΔV_i represents the voltage value at time $i\Delta t$. Roughness R_a is a global characterization of the scale in voltage fluctuation. The power spectrum, additionally, allows detecting not only the main frequencies contained in the voltage oscillation, but also the change in behavior of the noise background on which the main frequencies appear as pronounced peaks. Here ''noise'' is to be understood as processes occurring at time scales much smaller than those resolved in the experimental measurement but which can be effectively described through random variables, since their details are not relevant in the resolved scale.

In order to avoid masking this characteristic noise signal by an actually pure random fluctuation, 5 up to 8 power spectra were considered for each case and wear stage; i.e., 5-8 time-voltage series were measured for each

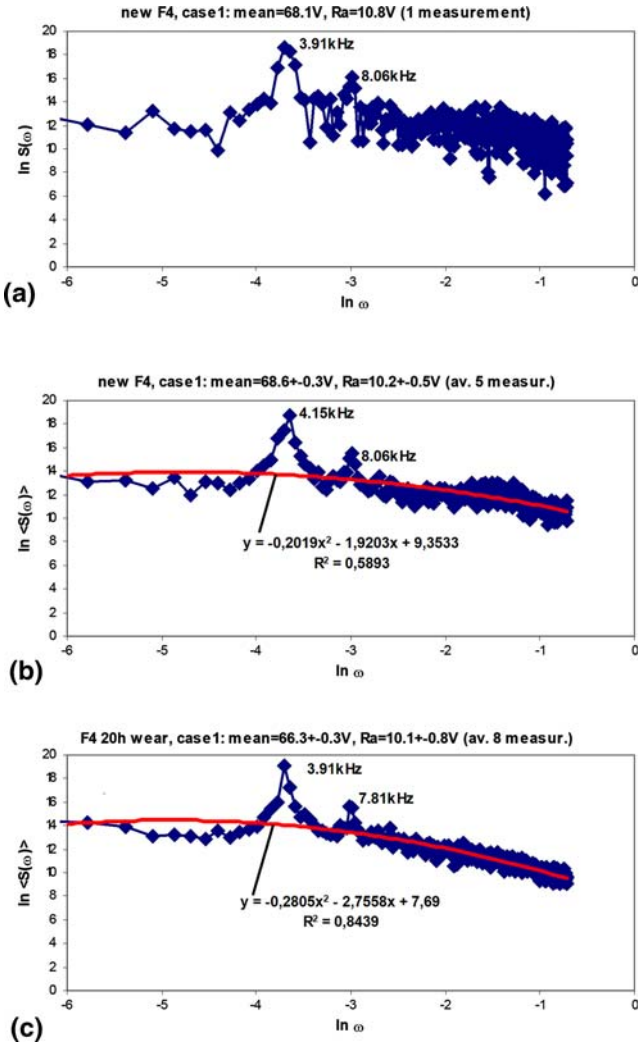

Fig. 1 For case 1, (a) (*above*) power spectrum from only one time-voltage series and with a new anode. (b) Averaged power spectra with new anode; and (c) (*below*) after 20 h. *Curves*: fitting to a second-order polynomial

considered case. The average $\langle S(\omega)\rangle$ of the corresponding power spectra was calculated, with a resulting enhancement in the structure of the high frequency range (Fig. 1a and b). Further, in order to filter out those Fourier components, which cannot correspond to any relevant physical effect (since too fast), an upper cutoff of 80 kHz has been implemented. Although theoretically such cutoff could be chosen up to a frequency of 250 kHz (corresponding to twice the smallest time scale measured), above 100 kHz the power spectrum displays a nearly horizontal progression, without any kind of structure (corresponding thus to white noise) and between 80 and 100 kHz the electric power unit produces an artificial peak (Fig. 2). The repeated series measurement allows also estimating the standard deviation for the mean voltage and the roughness (Eq. 2).

On the one hand, the resulting averaged power spectrum displays two main peaks where the second lower peak corresponds to the harmonic value (double frequency) of the first one within the frequency resolution determined by $\Delta t = 2$ μs (Fig. 1), and on the other hand, the high frequency FFT components (above frequency $f = 20$ kHz, range $-2 \le \ln\ \omega \le -1$ with $\omega = 2\pi f$ measured in 1 $\mu s^{-1} = 10^3$ kHz) are gradually suppressed with increasing wear, feature particularly pronounced in the Ar/H_2 case. This latter effect can be quantitatively described by the fitting of the whole averaged power spectrum (in double logarithmic representation and up to a frequency of 80 kHz) to a second-order polynomial (since the main peaks yield a negligible contribution to the fitting compared to the noise background), as follows:

$$\ln \langle S(\omega)\rangle = c_0 + c_1 \ln \omega + c_2 (\ln \omega)^2 \qquad \text{(Eq 3)}$$

with c_0, c_1, and c_2 the fitting constant parameters. The curvature change is characterized through the evolution of the (negative) parameter c_2.

The results are presented in Table 2. With increasing wear (denoted by the number of operation hours), there is no appreciable evolution in the localization of the two main frequency peaks: these remain at the same values. Only for a significantly worn anode the height of the second harmonic is strongly decreased. Hence, to consider only the evolution in the voltage spectrum main peaks does not yield an accurate form to track the anode wear. This conclusion holds even for the Ar/H_2 case, where a more efficient anode erosion, and thus a stronger arc root anchoring, is to be expected due to the more pronounced constriction of the plasma core (Ref 9).

In the Ar/H_2 case (case 1) nevertheless, the measured voltage roughness and the curvature of the high frequency noise in the power spectrum do markedly change with growing wear. Since also the mean voltage slightly changes with increasing anode erosion, in order to compare different situations to each other a normalized roughness ξ_a is defined as the quotient between the voltage roughness R_a and the mean voltage ΔV_{ave} as follows

$$\xi_a = 100 \frac{R_a}{\Delta V_{ave}} \qquad \text{(Eq 4)}$$

The evolutions of power spectrum curvature and normalized roughness are represented in Fig. 3 for the Ar/H_2 flow (case 1 of Table 1). For this case, with increasing wear the power spectrum's c_2 fitting parameter also exhibits monotonic increase whereas the normalized roughness, after reaching a maximum, decreases; the correlation coefficient of both parameters to the number of operation hours is quite good (Fig. 3). The decrease of c_2 results from the gradual suppression of the voltage's Fourier components in the range above 20 kHz. Since the voltage fluctuation is due to the motion of the arc root along the anode surface, such strength decrease in high frequency indicates a growing anchoring of the arc root at the anode wall due to its erosion when operating in case 1 conditions. The second effect, the decrease in the normalized roughness ξ_a after a maximum in case 1, can be used to determine the anode erosion stage when operating with Ar/H_2: after measuring ξ_a initially (when the anode wall is new), the normalized roughness is

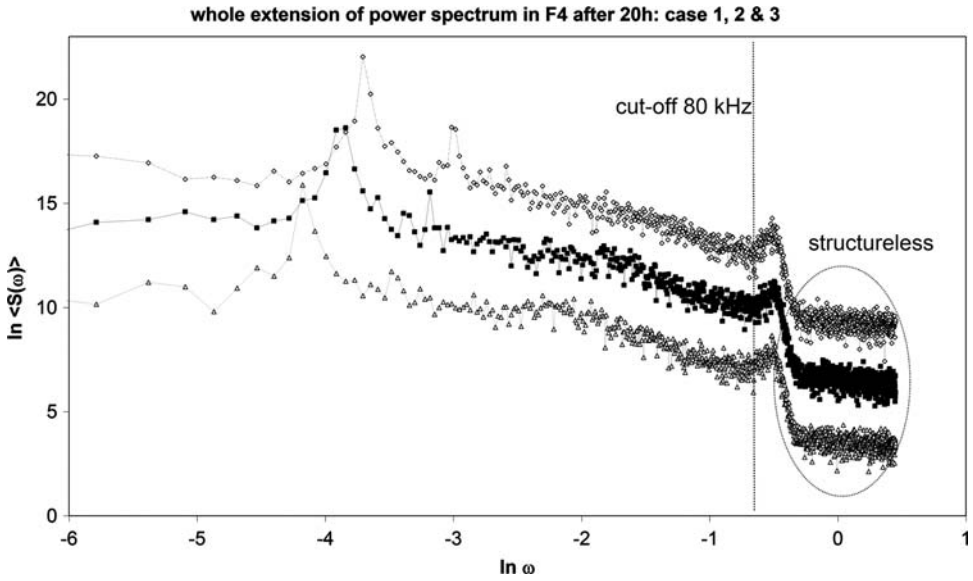

Fig. 2 Average power spectrum after 20 h for the three cases considered. For frequencies above 80 kHz, the spectrum contains an artificial peak and above 100 kHz becomes rather horizontal, characteristic of a white noise. The first and third spectrums are displaced by three units vertically, upwards and downwards respectively

Table 2 Evolution of mean voltage (ΔV_{ave}), roughness (R_a), power spectrum curvature ($|c_2|$), and main peak frequencies for different wear stages (in operation hours) in a F4 torch for the cases given in Table 1

	Case	ΔV_{ave}, V	R_a, V	$\|c_2\|$	Main freq., kHz
New	1	68.6 ± 0.3	10.2 ± 0.5	0.2019	4.15, 8.06
	2	65.0 ± 0.5	11.4 ± 0.4	0.2919	3.42, 6.59
	3	66.8 ± 0.5	10.0 ± 0.3	0.2272	2.44, 5.13
5 h	1	67.8 ± 0.2	11.3 ± 0.6	0.2289	4.15, 8.06
	2	65.4 ± 0.4	11.6 ± 0.4	0.3154	3.42, 6.59
	3	67.3 ± 0.7	10.4 ± 0.5	0.2425	2.69, 5.13
10 h	1	69.1 ± 0.5	11.1 ± 0.5	0.2268	3.91, 8.06
	2	66.6 ± 0.4	11.3 ± 0.2	0.2958	3.42, 6.59
	3	67.6 ± 0.3	10.3 ± 0.3	0.2475	2.44, 5.13
15 h	1	67.3 ± 0.7	10.2 ± 0.6	0.2738	3.91, 8.06
	2	65.8 ± 0.6	11.4 ± 0.4	0.3501	3.42, 6.59
	3	67.3 ± 0.2	9.9 ± 0.4	0.2516	2.44, 5.13
20 h	1	66.3 ± 0.3	10.1 ± 0.8	0.2805	3.91, 7.81
	2	66.2 ± 0.2	11.3 ± 0.4	0.2847	3.42, 6.59
	3	67.4 ± 0.4	9.5 ± 0.3	0.2918	2.44, 4.88
25 h	1	65.8 ± 0.3	9.6 ± 0.7	0.3157	3.91, 7.81
	2	66.2 ± 0.2	11.3 ± 0.4	0.3236	3.42, 6.59
	3	67.1 ± 0.3	9.1 ± 0.3	0.2921	2.44
>25 h	1	65.0 ± 0.2	8.5 ± 0.2	0.3063	3.91, 6.59
	2	64.4 ± 0.5	10.1 ± 0.4	0.3155	3.42, 6.35
	3	64.8 ± 0.5	9.5 ± 0.6	0.3195	2.69

For the two last wear stages, case 3 displays almost only one main frequency

measured periodically and as soon as it goes below its initial value, the anode wall can be considered to start eroding appreciably. This effect should be accompanied by the steady increase in the power spectrum's curvature.

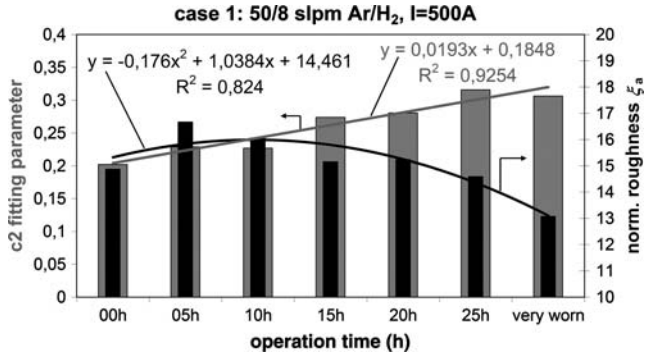

Fig. 3 Time evolution of power spectrum curvature $|c_2|$ and normalized voltage roughness ξ_a for the case 1 of Table 1

In cases 2 and 3 (data in Table 2), the two aforementioned effects are not so pronounced. A probable explanation for this absence is a shorter plasma core (in downstream direction), unable thus to reach the developing wall depression created by the arc during operation in case 1. For a given power and mass flow, the plasma arc adjusts itself to a radial and longitudinal size which minimizes the entropy production rate (Ref 9). For that, the heat transfer from the core to the anode wall, which is being cooled down externally, has to be reduced at most. The degree of core constriction is mainly controlled by the thermal conductivity of the plasma gas mixture at the flow temperature near the anode wall. Both H_2 and N_2 have a relative high thermal conductivity below 7000 K, due to the molecular dissociation (Ref 11). As such dissociation occurs at a lower temperature in the case of H_2, the resulting core constriction is more pronounced in this latter case.

Hence the Ar/N_2 case 2 can afford to expand a little bit more radially than in case 1 and thus does not require a longer core in longitudinal direction to store the power being injected into the torch (slightly lower than in case 1, see ΔV_{ave} in Table 2). Nevertheless, a shorter core means also that the location of the eroded depression being built in case 1 cannot be reached in case 2 (or only at the largest fluctuations). Thus arc root can move more freely. Additionally, the less radially constricted core in case 2 leads to a lower temperature within the core (higher mass density) and therefore a lower gas velocity for a given mass flow. Such decreased velocity ''pushes'' more slowly the arc downstream and yields a lower fluctuation frequency as in case 1 (compare main peaks in Table 2). In case 3, for its part, the mass flow already lower than in case 1 and 2 leads also to a lower gas velocity and its directly responsible for the lower values in the main peaks of the spectrum.

Finally, it is worth noting that the frequency range, where the gradual suppression of power spectrum components is observed, corresponds well to that for an arc core motion on the anode wall in azimuthal direction; i.e., without moving further downstream. Such a motion is created by the swirl component in the gas velocity, calculated from the injection velocity V_{inj} of the gas into the torch. It will be assumed that this swirl component remains almost unchanged in downstream direction. Since the maximal length scale for this motion before being interrupted is about half the torch nozzle circumference, the lowest time scale τ can be expressed as follows:

$$\frac{1}{\tau} \sim \frac{V_{inj} \sin \theta_{swirl}}{\pi \, r_{noz}} \qquad \text{(Eq 5)}$$

This corresponds to a value of about 1.5 kHz for a swirl angle of $\theta_{swirl} = 30°$, a torch nozzle radius $r_{noz} = 3$ mm and a velocity of $V_{inj} = 26$ m/s (which corresponds to 50 slpm Ar). A shorter covered arc of about 15° in azimuthal direction (Ref 2) leads to fluctuation frequencies in the order of 15 kHz.

As already mentioned, for the Ar/H_2 case where the anode wear is the strongest, the evolution of the normalized voltage roughness ξ_a can be used as a reliable criterion for anode erosion when after an initial increase, the value of ξ_a starts decreasing and descends below its start value. A further characterization for the onset of anode erosion is discussed in the following section.

3. Curvature Analysis of Particle Temperature Distributions

As described previously the azimuthal symmetry of the arc root movements is distorted by anode erosion. Through this, transfer of kinetic and thermal energy to the injected powder particles is affected. Therefore in-flight measurements of particle characteristics should give information on the significance of this impact. These measurements were performed by a DPV-2000 diagnostic system (TECNAR Automation Ltd., St-Bruno, QC, Canada) on a 7×7 point grid in a *x*,*y*-plane normal to the gun axis at the spray distance. The grid was dimensioned 12×12 mm^2 and measurement time was 5 s per grid point so that up to approximately 500 particles were captured ensuring sufficient statistical support of the mean values. The powder was an Aluminate with particle diameters of +32 −80 μm; the F4 gun was operated at standard parameters (current 660 A, power 41 kW and plasma gases 40/10 slpm Ar/H_2).

Figures 4 and 5 show the measurement results using a F4 gun equipped with a new or with an eroded anode, respectively. The comparison of the measured temperatures indicates that for the worn state the maximum is shifted upwardly and the distribution appears distorted. In order to quantify the latter effect, the values were approximated by a second order regression polynomial *R* yielding reasonable coefficients of correlation (i.e., $r^2 > 0.85$):

$$R(x,y) = \sum_{i=0}^{2} \sum_{j=0}^{2} a_{ij} x^i y^j \qquad \text{(Eq 6)}$$

where x is the horizontal and y the vertical coordinate, respectively, and a_{ij} are the polynomial coefficients. Subsequently the curvature characteristics of the regression surface are evaluated at the maximum point (x_0, y_0). Here the surface normal vector is vertical upon the *x*-*y*-plane, which is expressed by:

$$\left.\frac{\partial R}{\partial x}\right|_{\substack{x=x_0 \\ y=y_0}} = 0, \quad \left.\frac{\partial R}{\partial y}\right|_{\substack{x=x_0 \\ y=y_0}} = 0 \qquad \text{(Eq 7)}$$

These conditions lead to a nonlinear system of equations, which is to be solved numerically for the maximum

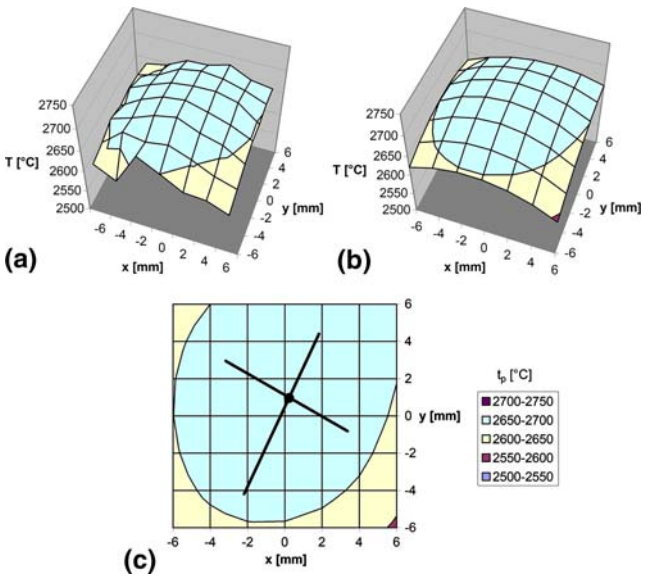

Fig. 4 Measured distribution of particle temperatures in spray distance (a), regression (b) and curvature analysis (c); F4 gun with *new* anode

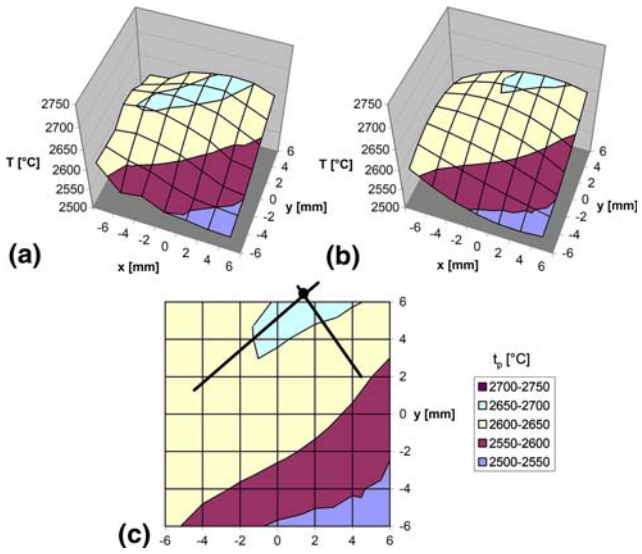

Fig. 5 Measured distribution of particle temperatures in spray distance (a), regression (b) and curvature analysis (c); F4 gun with *eroded* anode

coordinates (x_0, y_0). In the neighborhood of this point the surface can be approximated by a Taylor series expansion containing two quadratic and one bilinear component. Turning the coordinate system, there is one orientation at which the latter vanishes and the two quadratic components become maximum and minimum, respectively. This complies with the diagonalization of the coefficient matrix. The remaining components represent two superposed cylinder surfaces with their axes being perpendicular to each other. The reciprocal cylinder radii are called main curvatures and their alignments are the main curvature directions. To calculate them, some differential geometric relationships are used. Initially, the coefficients of the first fundamental form describing the metric characteristics of the surface are to be determined. It can be expressed as follows:

$$E = 1 + \left(\frac{\partial R}{\partial x}\right)^2, \quad F = \frac{\partial R}{\partial x}\frac{\partial R}{\partial y}, \quad G = 1 + \left(\frac{\partial R}{\partial y}\right)^2 \qquad \text{(Eq 8)}$$

Furthermore the coefficients of the second fundamental form describe the curvature characteristics of the surface and correspond to:

$$L = \frac{\left(\frac{\partial^2 R}{\partial x^2}\right)}{\sqrt{EG - F^2}}, \quad M = \frac{\left(\frac{\partial^2 R}{\partial x \partial y}\right)}{\sqrt{EG - F^2}}, \quad N = \frac{\left(\frac{\partial^2 R}{\partial y^2}\right)}{\sqrt{EG - F^2}} \qquad \text{(Eq 9)}$$

Both the main curvature directions $(\lambda, \mu)_{I,II}$ being normal to each other can be calculated from the following quadratic equation:

$$\lambda^2(FN - GM) + \lambda\mu(EN - GL) + \mu^2(EM - FL) = 0$$

The absolute curvature values k_I and k_{II} are obtained from the Gaussian curvature as follows:

$$K = \frac{LN - M^2}{EG - F^2} = k_I k_{II} \qquad \text{(Eq 10)}$$

and from the mean curvature it comes:

$$H = \frac{LG - 2FM + EN}{2(EG - F^2)} = \frac{1}{2}(k_I + k_{II}) \qquad \text{(Eq 11)}$$

via the following quadratic equation:

$$k^2 - 2Hk + K = 0 \qquad \text{(Eq 12)}$$

The maxima points and the main curvature directions are indicated in the contour plots in Figs. 4c and 5c. For the new anode the absolute curvatures are of the same magnitude, so the contour ellipses are approximately circular shaped. In contrast the plots of the eroded state show stretched contour ellipses due to the significant difference of the main curvatures. Thus, the ratio of the main curvatures is a significant indicator for anode erosion. It is proposed to use the following criterion to estimate quantitatively relevant anode erosion:

$$\left|\frac{k_I - k_{II}}{k_I + k_{II}}\right| > 0.5 \qquad \text{(Eq 13)}$$

In the examples shown above this characteristic value is 0.2 (<5 h) for the new anode and 2.0 for the eroded anode (''very worn''), respectively. The proposed threshold of 0.5 may be adapted individually to specific applications whereto some more experience is still to be collected.

Particle velocity distributions are also affected by anode erosion, but the impacts on the particle temperatures are more obvious. Hence, curvature analysis of particle temperature distribution is a feasible method to estimate the wear state of one-cathode plasma torches. The results also emphasize that anode erosion is a variable strongly influencing the in-flight particle state and thus the characteristics of the coatings.

4. Conclusions

Two different diagnostic procedures have been presented to estimate the wear stage of the anode in a single cathode plasma torch. The first one is based on the power spectrum analysis of the torch voltage and tracks the wear through the steady increase in the suppression of high frequency components. In the second technique, the development of anode erosion is mirrored in the symmetry loss for the spatial distribution in the measured temperature of particles injected into the plasma.

During thermal spray production, monitoring the wear state of the electrodes by voltage measurement method will be the easiest way for many applications. It can be done continuously without interrupting the process. However, a series of measurements during the lifetime of the electrodes is necessary as the detection of wear is based on the evaluation of the development of the measured values. Furthermore, it is necessary to have available a sequence of measurements under similar spray

parameters. In contrast, the alternative method based on particle temperature measurements yields an absolute criterion to assess the state of the gun. Only one set of measurement at any one time is needed. This may be an advantage if there is no sequence of measurements available.

Acknowledgment

The authors would like to thank Mr. K.-H. Rauwald (IEF-1, Forschungszentrum Jülich, Germany) for his support in performing the measurements.

References

1. J.F. Coudert, M.P. Planche, and P. Fauchais, Characterization of D.C. Plasma Torch Voltage Fluctuations, *Plasma Chem. Plasma Process.*, 1996, **16**(Suppl. 1), p 211S-227S
2. Z. Duan and J. Heberlein, Arc Instabilities in a Plasma Spray Torch, *J. Thermal Spray Technol.*, 2002, **11**(1), p 44-51
3. W. Zhao, K. Tian, H. Tang, D. Liu, and G. Zhang, Experimental Studies on the Unsteadiness of Atmospheric Pressure Plasma Jet, *J. Phys. D: Appl. Phys.*, 2002, **35**, p 2815-2822
4. J.F. Bisson, B. Gauthier, and C. Moreau, Effect of Plasma Fluctuations on In-Flight Particle Parameters, *J. Thermal Spray Technol.*, 2003, **12**(1), p 38-43
5. J.F. Bisson and C. Moreau, Effect of Plasma Fluctuations on In-Flight Particle Parameters: Part II, *J. Thermal Spray Technol.*, 2003, **12**(2), p 258-264
6. L. Leblanc and C. Moreau, The Long-Term Stability of Plasma Spraying, *J. Thermal Spray Technol.*, 2002, **11**(3), p 380-386
7. M. Vyšohlíd and J. Heberlein, Investigation of Arc Voltage Fluctuation in a Plasma Torch SG-100 operated with Ar/H_2, *Thermal Spray 2004: Advances in Technology and Application*, ASM International, May 10-12, (Osaka, Japan), ASM International, 2004
8. H. Weckmann, S. Fiebig, A. Syed, and J. Arnold, Investigation of Time-Dependent Instabilities of Plasma Spraying Process Using Online Diagnostic Systems, *Building on 100 Years of Success*, B.R. Marple, M.M. Hyland, Y.-C. Lau, R.S. Lima, and J. Voyer, Eds., May 15-18, (Seattle, WA, USA), ASM International, 2006
9. K. Ramachandran, J.-L. Marqués, R. Vaßen, and D. Stöver, Modelling of Arc Behaviour inside a F4 APS Torch, The Long-Term Stability of Plasma Spraying, *J. Phys. D: App. Phys.*, 2006, **39**(15), p 3323-3331
10. W.H. Press, B.P. Flannery, S.A. Teukolsky, and W.T. Vettering, Numerical Recipes in C, 2nd ed Cambridge University Press, Cambridge (UK), 1992
11. M.I. Boulos, P. Fauchais, and E. Pfender, Thermal Plasmas. Fundamentals and Applications. Plenum Press, New York, NY, USA, 1994